

Effect of Sulfur Coverage on Fe(110) Adhesion: A DFT Study

Michelle J. S. Spencer, Ian K. Snook, and Irene Yarovsky*

Applied Physics, RMIT University, GPO Box 2476V, Victoria, 3001, Australia

Received: October 28, 2004; In Final Form: February 13, 2005

The effect of adsorbed S at different coverages on the adhesion of Fe(110) surfaces in match and mismatch is examined using density functional theory (DFT). S is adsorbed in atop, bridge, and 4-fold hollow sites on one side of the interface in $c(2 \times 2)$ and $p(1 \times 1)$ arrangements, corresponding to coverages of 1/2 and 1 monolayer, respectively. The calculated adhesion energy values at different interfacial separations are fitted to the universal binding energy relation [Rose et al. *Phys. Rev. B* **1983**, *28*, 1835], and the effect of the S coverages on the adhesive strength is analyzed. The effect of relaxation of the interfaces at equilibrium is also investigated, and the resulting interfacial structures and related magnetic and charge density properties are compared.

1. Introduction

The use of metals in many industrial processes is greatly influenced by the presence of impurities, since they affect the bulk and surface properties of the metal. In the case of metallic iron (Fe), one of the most common impurities is sulfur (S), which has been shown to affect the adhesion, friction, wear behavior, and grain boundary cohesion of Fe.¹

It is often difficult in experimental studies to control the type and level of contaminants that are present, making it hard to determine how a specific impurity affects the property of a metal being investigated. By using a theoretical approach, the level of contamination and type of impurity can be precisely controlled, allowing a systematic study of the impurity's effect on the structure, electronic properties, and magnetic properties to be performed.

We have previously examined adhesion between clean bulk-terminated Fe (100), (110),² and (111)³ surfaces in match and mismatch using density functional theory (DFT). We have also examined the effect of adsorbed S, at the experimentally observed surface coverage of 1/4 monolayer (ML) in a $p(2 \times 2)$ arrangement, on the adhesion of Fe(110) surfaces in match and mismatch.⁴

The effect of S impurity on Fe adhesion has been examined experimentally^{1,5,6} at various coverages and on different Fe surfaces. There appears to be some conflicting experimental evidence as to the surface effect of the adsorbed S and whether it increases or decreases the Fe adhesion.

Specifically, Buckley¹ examined the effect of S (segregated to the surface in a $c(2 \times 4)$ arrangement and 1/4 ML coverage) on the adhesion of Fe(110). Buckley found that the S appreciably decreased the adhesive strength of the interface.

Later, Hartweck and Grabke^{5,6} examined the effect of segregated S on the adhesion of polycrystalline Fe surfaces (zone-melted Fe) at different coverages. In contrast to the previous study, they found that the S actually increased the strength of adhesion compared to that of the clean surfaces at submonolayer concentrations, showing a maximum in the adhesive force at an estimated S coverage of 0.6 ML (S atoms/

Fe atoms). At coverages greater than 1 ML, S reduced the strength of adhesion compared to the clean surfaces. As S has been shown previously to cause embrittlement of Fe⁵ when present at grain boundaries at the same concentrations, they suggested that the difference in their adhesion experiments from those performed previously could be explained by processes that occur at the grain boundary. As the decrease in grain boundary cohesion occurs after heating, they suggest that the heating causes a reconstruction to occur at the interface. In contrast, the lower temperature and short contact time for the adhesion experiments do not allow sufficient time for such a reconstruction to occur. They suggest that further work should be done to confirm such an explanation. We could not find any evidence in the literature of such further work.

Moreover, in all the experimental studies, no information was obtained on the actual structure of the interface or how the S impurity affects the fundamental electronic and magnetic properties of the interface.

Our previous work allowed us to quantitatively describe the adhesion properties of clean Fe (100), (110), and (111) interfaces and to compare the relative adhesive strength of the interfaces. To compare the relative strength of adhesion between different surfaces, we have calculated the adhesion energy values of the interfaces at different interfacial separations. Fitting the universal binding energy relation (UBER)⁷ to these values allowed us to obtain the work of separation, W_{sep} , which is defined as the work required to separate an interface to infinity, ignoring relaxation and diffusion processes.^{8,9} The equilibrium interfacial separation, d_0 , and the screening factor, l , were also obtained for the quantitative comparison of adhesion.

In the present study we examine the effect of different coverages of atomic S on the adhesion of Fe(110) surfaces in match (epitaxy) and mismatch (out of epitaxy) using DFT within the plane-wave pseudopotential method. The effect of S adsorbed in three adsorption sites (atop, bridge, and 4-fold hollow) at two different arrangements, $c(2 \times 2)$ and $p(1 \times 1)$, corresponding to coverages of 1/2 and 1 ML, respectively, is investigated. We examine the calculated adhesion energy curves and changes in electron density distribution and magnetic properties at different interfacial separations. The results are compared to the findings obtained previously for the clean

* Corresponding author. Telephone: +61 3 9925 2571. Fax: +61 9925 5290. E-mail: irene.yarovsky@rmit.edu.au.

matching and mismatching Fe(110) interfaces² and the 1/4 ML coverage S-contaminated Fe(110) interfaces.⁴

2. Method

2.1. Computational Details. Our calculations were performed using the Vienna Ab initio Simulation Package (VASP),^{10–12} which performs fully self-consistent DFT calculations to solve the Kohn–Sham equations.¹³ The generalized gradient spin approximation (GGA), using the functional of Perdew and Wang (PW91),¹⁴ was employed. The electronic wave functions were expanded as linear combinations of plane waves, with a kinetic energy cutoff of 308.76 eV. *K*-space sampling was performed using the scheme of Monkhorst and Pack¹⁵ using a $6 \times 6 \times 1$ mesh, determined previously for cells of this size.¹⁶ The ultrasoft pseudopotentials for Fe and S as included in the VASP package¹⁷ were used for all calculations. Our previous work showed that this approach gives a good description of bulk, surface, and interfacial properties of Fe,^{2,3,18,19} FeS₂,^{20–22} and S/Fe(110).^{16,23} For the calculation of fractional occupancies of the relaxed interfaces, a broadening approach by Methfessel–Paxton²⁴ was used with order $N = 1$ and smearing width 0.1 eV. For accurate calculation of total energies and magnetic moment values of the interfaces at different separations, the tetrahedron scheme²⁵ was employed, using a Weigner–Seitz radius of 1.3 and 1.164 Å for Fe and S, respectively.

2.2. Interface Models. The Fe interfaces were constructed using our relaxed S/Fe(110) surface models determined previously,^{16,23} and represented adhesion between a relaxed S/Fe(110) surface and an unrelaxed clean Fe(110) surface. Such a model enabled a comparison with the previous study of adhesion between unrelaxed clean Fe(110) surfaces.² The previously obtained S/Fe(110) surface models²³ comprised five Fe layers with a S atom adsorbed in either an atop, bridge, or 4-fold hollow site on one side of the slab in the following arrangements: *c*(2 × 2) and *p*(1 × 1), corresponding to coverages of 1/2 and 1 ML, respectively. For the surface relaxation studies, the S and top three Fe layers were relaxed while the bottom two layers were kept fixed. These relaxed models were used in the present study to model a mismatching interface, where insertion of the vacuum spacer in the *z*-direction resulted in formation of the interface and interfacial separations were sampled by adjusting the size of the vacuum spacer. The mismatching interface models are shown in Figure 1 with S adsorbed in an atop site at different coverages. Surface A is the relaxed S/Fe(110) surface, while surface B is the unrelaxed clean Fe(110) surface. To model matching interfaces, a sixth layer was added to the bottom of the relaxed five-layer model shown in Figure 1. It should be noted that we define matching and mismatching interfaces according to the geometry of the interface formed when the S is absent. The interfacial separation is defined as the distance between the topmost Fe atoms on each surface. The total energy of each interface was calculated for at least 10 different interfacial separations between 12 and ~2 Å.

The work of separation, W_{sep} , of each interface was determined from a plot of the calculated adhesive energy versus interfacial separation, where the adhesive energy, $E_{\text{ad}}(d)$, is obtained as

$$E_{\text{ad}}(d) = (E(d) - E(\infty))/A \quad (1)$$

where $E(d)$ is the total energy of the system calculated at interfacial separation d , $E(\infty)$ is the total energy at infinite separation, and A is the unit cell surface area in the *x*, *y* direction.

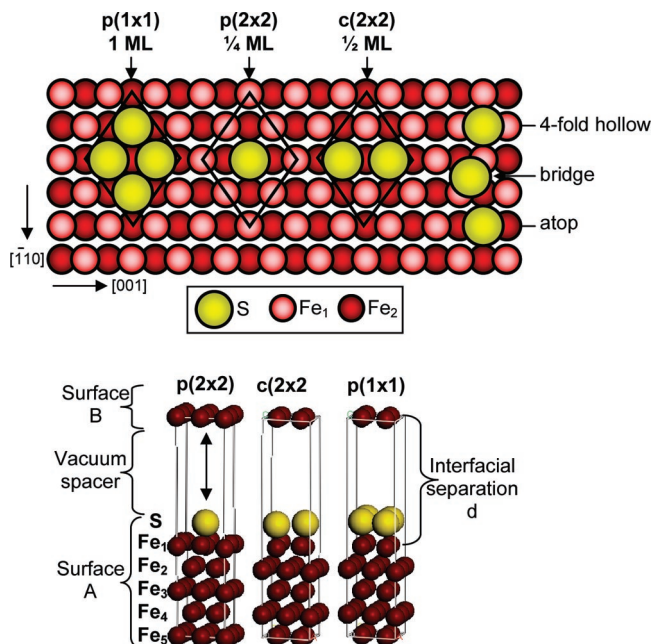


Figure 1. Top and side views of unit cells used to represent the different S-contaminated interfaces. (Only the atop site is shown for the side view.)

The well depth of this curve at the equilibrium separation, E_0 , is equivalent to the work of separation.²

The UBER⁷ was fitted to the calculated adhesion energy values, from which the following parameters were obtained analytically: E_0 , the well depth at the equilibrium interfacial separation, d_0 ; l , the screening length, which may be interpreted as the approximate distance over which electronic forces act. The peak interfacial stress (per unit area of interface), $\sigma_{\text{max}} = 2E_0/le$, where e is the base of the natural logarithm, was also calculated.

Further calculations were performed on the interface models at their equilibrium separation. All atoms were allowed to relax in the *x*-, *y*-, and *z*-directions, while the cell volume was also allowed to change, to examine the effect of relaxation on adhesion, electronic properties, and magnetic properties of the interface.

3. Results and Discussion

3.1. Adhesion Energy curves and UBER parameters. It is useful to first have a clear understanding of the geometry at the interface of each system before comparing their related properties. For the mismatching interfaces, the S bonds to the same adsorption site on both surface A (relaxed) and surface B (unrelaxed). It should be noted that S has been shown at most coverages to cause the Fe surface atoms within the same layer to relax by different amounts, leading to buckling of the layer.^{16,23} Since the clean surface is not buckled,¹⁸ the modeled interface is not symmetrical across the interface boundary.

For the matching interfaces, the S bonds to different sites on surfaces A and B. We will identify the interface by the position of the S on surface A. For the atop interfaces, (i.e., S bonds to an atop site on surface A) S bonds to a 4-fold hollow site on surface B. For the bridge interfaces, the S actually bonds to the bridge sites of both surfaces; however, the Fe atoms forming the bridge site on the different surfaces are perpendicular to each other. For the 4-fold hollow interfaces, S bonds to an atop site on surface B. Hence, the atop and 4-fold hollow matching interfaces have the same geometry except that surface A is relaxed while surface B is unrelaxed.

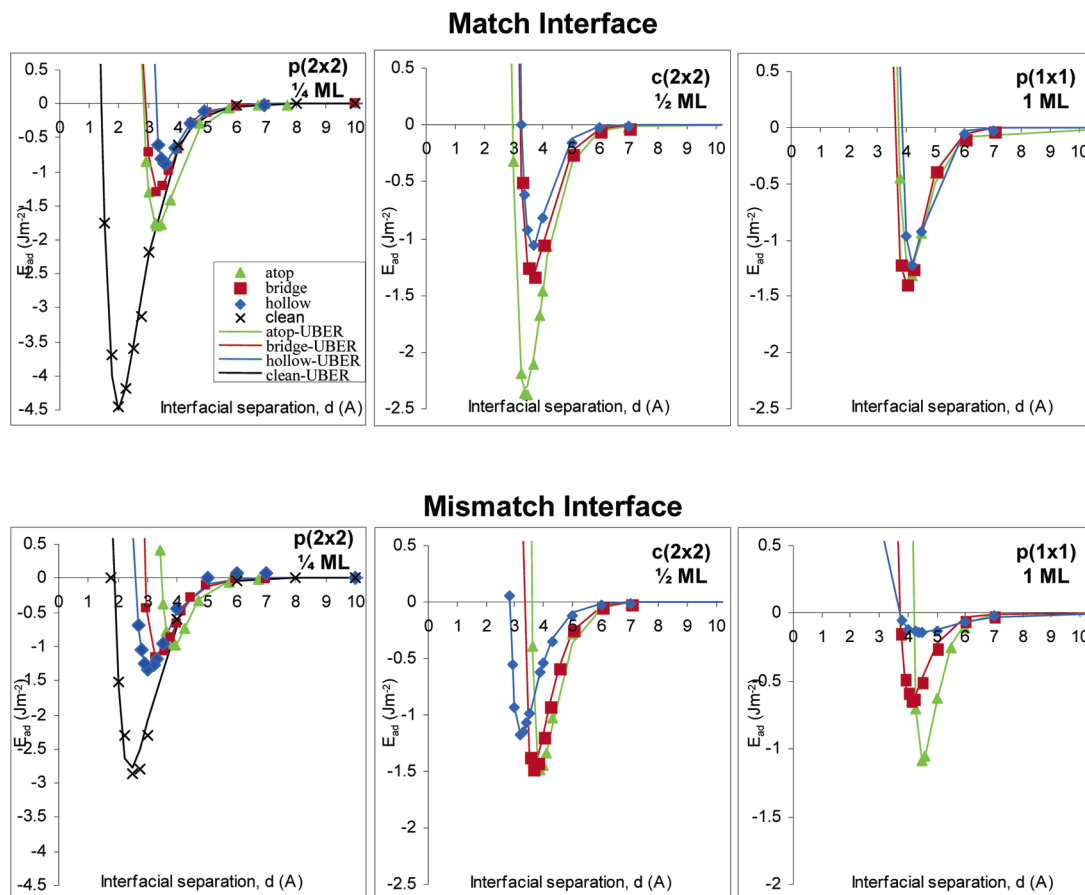


Figure 2. Calculated adhesion energy curves and fitted UBER for matching and mismatching Fe(110) interfaces with S contaminant at the different arrangements and coverages indicated. The corresponding curves obtained previously for the clean interfaces² as well as the $p(2 \times 2)$ -S-1/4 ML⁴ plots are also shown. Note the different y-axis scales for these plots.

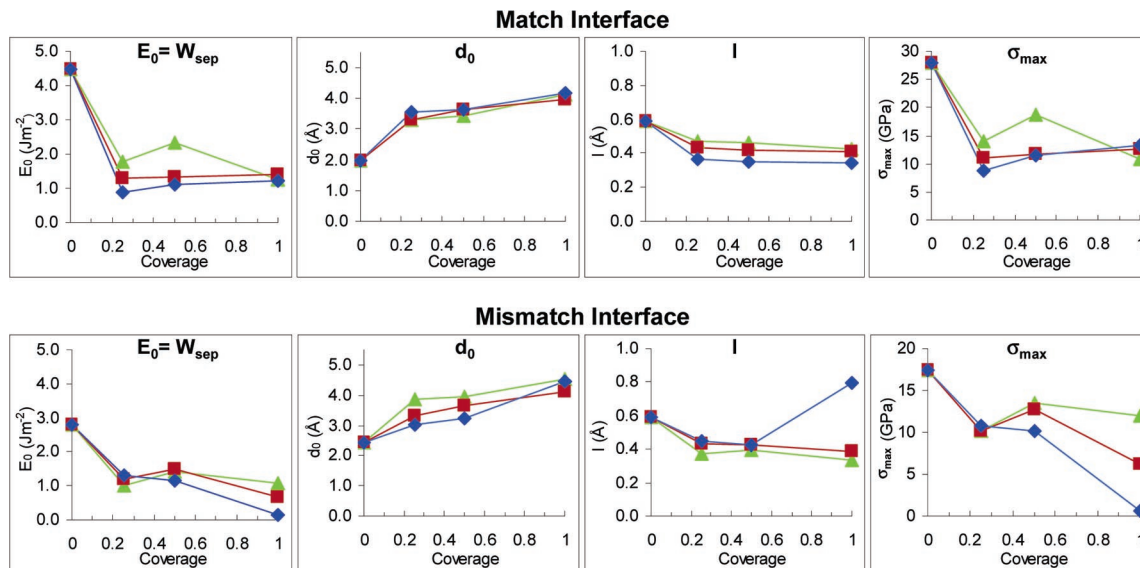


Figure 3. Calculated UBER parameters $E_0 = W_{\text{sep}}$, d_0 , l , and σ_{max} , for matching and mismatching Fe(110) interfaces as a function of S contaminant coverage (ML). Symbols indicating different S adsorption sites are the same as in Figure 2.

The calculated adhesion energy and fitted UBER curves for S adsorbed in atop, bridge, and 4-fold hollow sites at matching and mismatching interfaces are shown in Figure 2, along with the curves obtained previously for the clean interfaces.² The fitted UBER parameters are presented in Figure 3 as a function of coverage.

As seen in Figure 2, the UBER provided a good fit to all curves, which was also reflected in the R^2 values which were

all > 0.99 . Comparison of the calculated W_{sep} values of the S-contaminated interfaces with those obtained for the clean matching and mismatching Fe(110) interfaces² shows that at all coverages and sites, as well as in both match and mismatch orientations, S decreases the adhesion. This is in agreement with the earlier experimental work of Buckley.¹

The relative strength of the S-contaminated interfaces is affected differently according to the S adsorption site, the

coverage, and the interface alignment. The strongest S-contaminated matching interface forms when S is adsorbed in an atop site at 1/2 ML coverage. The strongest mismatching interface forms when S is adsorbed in bridge sites at 1/2 ML coverage, with the atop interface at this coverage being almost as strong; neither of these interfaces is as strong as the matching interface, though.

At all S coverages, the weakest matching interfaces are formed when S is adsorbed in 4-fold hollow sites. The interfacial strength increases slightly when S is adsorbed in bridge sites and is again slightly stronger for S adsorbed in atop sites, with the only exception being for the monolayer coverage (1 ML) where the bridge interface is slightly stronger than the atop. This relative order is different from the isolated S-contaminated surface stability which decreased from the 4-fold hollow to the bridge and then to the atop contaminated site^{16,23} except for at 1 ML, where all three sites were of almost equal stability. The relative stabilities of the S-contaminated surfaces play a part in the calculated W_{sep} of the interfaces, as the adhesion energy is calculated by subtracting the total energy of the isolated surfaces (one clean and one S-contaminated surface) from the total energy of the interface at each separation. As we showed previously for the 1/4 ML S-contaminated atop and 4-fold hollow matching interfaces,⁴ the difference in total energy of the interfaces at equilibrium was <0.007%, but the W_{sep} of the atop interface was more than twice as large as that of the 4-fold hollow interface. As the clean surface is identical for both cases and the S-contaminated atop surface is less stable than the S-contaminated 4-fold hollow surface, the atop interface will have a larger W_{sep} value. The same applies to the 1/2 ML coverage. At 1 ML, however, the difference in stability of the atop and 4-fold hollow S-contaminated isolated surfaces is much smaller,²³ and with the difference in total energy of the interfaces still being within the computational error, the difference in calculated W_{sep} is smaller than it is at the other coverages.

The W_{sep} of the atop, bridge, and 4-fold hollow interfaces is found to vary with increasing S coverage as follows. As the coverage is increased from 1/4 to 1/2 ML, the W_{sep} increases where it is at a maximum and remains almost constant at 1 ML for the bridge and 4-fold hollow sites, while decreasing for the atop site. At 1 ML the strength of the interfaces varies by 0.16 J m⁻² among all three sites.

For the mismatching interfaces (Figure 3), the difference between the W_{sep} values for each site at the different coverages is smaller than that for the matching interfaces, except for the 1 ML coverage where the W_{sep} values differ by 0.95 J m⁻². In fact, the W_{sep} for the 4-fold hollow site at this coverage is 0.14 J m⁻², indicating that the interface is weak. Similar to the matching interfaces, S increases the W_{sep} as the S coverage is increased from 1/4 to 1/2 ML, before decreasing at 1 ML. Interestingly, the experimental study by Hartweck and Grabke⁶ measured the maximum adhesive force to occur at a S coverage of 0.6 ML, which is in line with our results.

The equilibrium separation values, d_0 , of the S-contaminated interfaces (Figure 3) show that S increases the equilibrium separation compared to the clean interfaces. Since we are measuring the interfacial separation as the distance between the topmost Fe atoms on each surface that forms the interface, it is not surprising, as S prevents the surfaces from approaching closer. For both matching and mismatching interfaces, the d_0 values increase with increasing S coverage. This is in line with the height of the adsorbed S on the isolated Fe(110) surface,^{16,23} where the S was found to sit higher above the surface when the adjacent S–S separation was smaller, as the interaction between

adjacent S atoms reduced their attraction to the surface. Therefore, as the S coverage is increased, and the S–S separation decreases, the S sits higher on the surface. This order is in line with the d_0 values of the interfaces, which are larger for the 1 ML coverage, followed by the 1/2 and 1/4 ML coverages. The relative d_0 values are also related to the adsorption sites on surface A and surface B. For the matching interfaces, there is little difference between the d_0 values of the different sites; however, for the mismatching interfaces the d_0 values are more spread out, being larger for the atop interfaces followed by the bridge and then 4-fold hollow interfaces. The only exception is for the 1 ML coverage, where the bridge d_0 is just slightly smaller than the 4-fold hollow site value. On the isolated S-contaminated surfaces,^{16,23} the height of S above the surface was found to decrease in the following order: atop, bridge, 4-fold hollow. As the mismatching interfaces comprise S bonding to two atop, two bridge, or two 4-fold hollow sites, it would be expected that the d_0 values would also be in the same order as on the isolated surface. This is indeed the case as seen in Figure 3. However, since the matching interfaces comprise different adsorption sites for surfaces A and B, the difference between the equilibrium separation values is not as large as the difference between the S distances for the isolated surfaces.

The calculated screening factor values, l , for the S-contaminated interfaces are found to be smaller than those for the clean interface, but do not vary much for different S coverages. The exception is the 4-fold hollow mismatching 1 ML interface, which has a much larger l value (0.8 Å), indicating that the interfacial attraction between these surfaces occurs over a larger range. However, as seen from the adhesion energy curve (Figure 2), the interaction between the surfaces forming this interface is weaker at all separations than that for the corresponding bridge and atop interfaces. Despite the small difference between the calculated l values for the different adsorption sites, the values tend to increase in size from the 4-fold hollow to bridge and atop sites for the matching interfaces. This order correlates to the height of the adsorbed S above surface A^{16,23} such that when S sits furthest from surface A (for the atop site), the surface starts interacting with surface B at a larger separation. For the mismatching interfaces, the size of the l values for different sites is found to be in the opposite order, indicating that the type of adsorption site on surface B also has an effect.

The calculated peak interfacial stress values, σ_{max} , for the S-contaminated matching interfaces were generally in line with the W_{sep} values, being largest for the strongest atop 1/2 ML matching interface. The mismatching interface σ_{max} values were also in an order similar to that of the W_{sep} values. It might be expected, though, that the 4-fold hollow 1 ML mismatching σ_{max} value would differ from the other interfaces because the W_{sep} and l values differ significantly from the other interfaces; however, the larger l value means the σ_{max} remains small.

3.2. Relaxed Interfaces at Equilibrium Separation. 3.2.1 *Adhesion Energy.* After relaxation of the interfaces at equilibrium separation, the adhesion energy and new equilibrium separation distance were calculated. The adhesion energy of the relaxed matching interfaces varied between 1.15 and 2.57 J m⁻².

Similar to the S-contaminated interfaces with 1/4 ML S coverage,⁴ relaxation was found to increase the calculated adhesion energy, with the order of the adhesion energy values of the unrelaxed matching interfaces remaining the same after relaxation and the strongest matching interface still being the atop 1/2 ML interface. The percentage change of the unrelaxed interface values can be seen in Table 1.

TABLE 1: Calculated Percentage Change (%) in Adhesion Energy, E_0 , and Interfacial Separation, d_0 , Values for the Interfaces at Equilibrium Separation after Relaxation

coverage	atop		bridge		hollow	
	E_0	d_0	E_0	d_0	E_0	d_0
Match						
<i>p</i> (2 × 2)	0.25	34.4	-30.3	50.0	-31.8	70.1
<i>c</i> (2 × 2)	0.5	10.4	7.2	7.9	0.8	4.5
<i>p</i> (1 × 1)	1	51.4	-2.1	62.0	-8.3	51.8
Mismatch						
<i>p</i> (2 × 2)	0.25	13.7	-19.7	19.3	-16.5	30.3
<i>c</i> (2 × 2)	0.5	9.2	-0.7	5.5	0.8	18.5
<i>p</i> (1 × 1)	1	45.0	-2.1	157.4	-6.8	945.7
						-17.1

The increase in E_0 values after relaxation was found to vary depending on the coverage, with the magnitude of the change generally being largest for the 1 ML coverage and smallest for the 1/2 ML coverage.

In contrast to the matching interfaces, the order of the mismatching interfaces did change after relaxation, showing the 1/4 ML 4-fold hollow interface rather than the 1/2 ML bridge interface to be the strongest. This interface is still weaker than the strongest atop interface, and the matching interfaces are still in general stronger than the corresponding mismatching ones.

The increase in E_0 after relaxation of the mismatching interfaces was found to be in the following order: 1/2 < 1/4 < 1 ML, with the 4-fold hollow 1 ML interface showing the largest increase, reflecting the effect that relaxation has on the interfacial strength.

Despite the increase in E_0 after relaxation of the S-contaminated interfaces, none of the interfaces showed a larger adhesion energy than the clean interfaces, in contrast to Hartweck and Grabke's^{5,6} experiments. It should be noted, however, that the experiments were performed above 0 K and the inclusion of temperature, which we have not performed here, should have an effect on the adhesion strength. In addition, their experiments were performed on polycrystalline samples, which comprise a mixture of different single-crystal faces; hence, it is possible that some other low index Fe interfaces may have stronger S-contaminated adhesion. At the same time, our findings agree with those of Buckley,¹ who did look specifically at Fe(110) adhesion.

3.2.2 Interfacial Separation and Geometry. After relaxation, the equilibrium interfacial separation, d_0 , was also recalculated and compared to the unrelaxed values (Table 1).

It was shown previously for a S coverage of 1/4 ML⁴ that d_0 decreased after relaxation of the matching interface. In the present study, it was found that, at S coverages of 1 ML, d_0 also decreased after relaxation for matching interfaces, but in contrast it was found to increase for the 1/2 ML coverage. The increase for the bridge and 4-fold hollow sites, however, was only <1% and is therefore not really inconsistent with the other coverages. The magnitude of the change in d_0 after relaxation was calculated to increase in the following order: 1/2 < 1 < 1/4 ML, which can generally be related to the size of the change in the relaxed E_0 values.

At 1/4 and 1/2 ML, the d_0 values are smaller than the unrelaxed clean value.² This seems surprising since it can be expected that S prevents the Fe surfaces from getting as close to each other. However, these small values are actually a result of buckling of the interface caused by relaxation and our definition of the interfacial separation.

It was shown previously for S adsorbed at a coverage of 1/4 ML⁴ that the atop and 4-fold hollow relaxed interfaces had the

same geometry and hence d_0 values. The differences for the unrelaxed interfaces arose because surface B was unrelaxed, while surface A was relaxed. At the other coverages examined here, the S again bonds to an atop site on one surface and a 4-fold hollow site on the other for both atop and 4-fold hollow interfaces and after relaxation the d_0 values only differ by <0.02 Å, indicating that the interfaces have the same geometry.

For the mismatching interface, relaxation was also shown previously to result in a decrease in d_0 at 1/4 ML.⁴ At the monolayer coverage, there is also a decrease in d_0 after relaxation, but for the bridge 1/2 ML coverage, a slight increase in d_0 value is observed, being only 0.8%. Unlike the matching interfaces, there is no clear trend in the magnitude of the d_0 change after relaxation; however, the change is generally larger for the smaller coverages. At these coverages, there are more Fe atoms that are not directly bonded to the S atom, which can relax by greater amounts, leading to a larger reduction in the interfacial separation.

After relaxation, the distance between the S atoms and the closest Fe atoms on either side of the interface (i.e., surface A and surface B) was also measured (see Figure 4).

As the volume of the interface models was allowed to change during the relaxation, some of the cell parameters were found to alter. These changes, however, were relatively small, being less than 0.35 Å in either the *x*- or *y*-direction for matching or mismatching interfaces. The largest increase in the *x*- and *y*-cell lengths was for the 1 ML coverage. These differences could partly explain the larger change in E_0 values after relaxation of these interfaces.

For the matching interfaces, the S–Fe distances to surface A and surface B were found to be different as expected, because the interfaces are not symmetrical across the interfacial boundary. For the atop matching interface, the shortest S–Fe distance on surface A (where S sits in an atop site) at the different coverages was found to be identical to that for S bonded to surface B in the 4-fold hollow interfaces, as S sits in an atop site on surface B for these interfaces. Similarly, the S–Fe distances to the alternate surface for the atop and 4-fold hollow interfaces at each coverage were also identical as S sits above a 4-fold hollow site on the alternate surfaces for these interfaces. For the bridge interfaces, the S–Fe distances were found to be identical for surface A and surface B, which is not surprising as the S atoms sit above a bridge site on both surface A and surface B.

For the mismatching interfaces, the S bonds to the same site on both surfaces (A and B) that form the interface. Similar to the relaxed mismatching interface with a S coverage of 1/4 ML,⁴ the S–Fe distances to surfaces A and B were found to be identical at the other coverages also. Hence only one value is shown in Figure 4. For all three sites, the S–Fe distance was found to increase with coverage, similar to the matching interfaces.

On the isolated S-contaminated Fe(110) surface, the S–Fe distances were found to be related to the S–S separation,^{16,23} being smaller when the S atoms were located further apart on the surface and larger when the S atoms were closer together, i.e., were interacting more strongly with each other. For the interfaces, on the other hand, the S–Fe distances appear to just increase with increasing coverage, indicating that the attraction between the Fe atoms on the two surfaces forming the interface competes with the S–Fe and S–S attractions. At smaller S coverages there are more Fe atoms which are not directly bonded to a S atom that can interact directly with Fe atoms on the other side of the interface, giving rise to the differences.

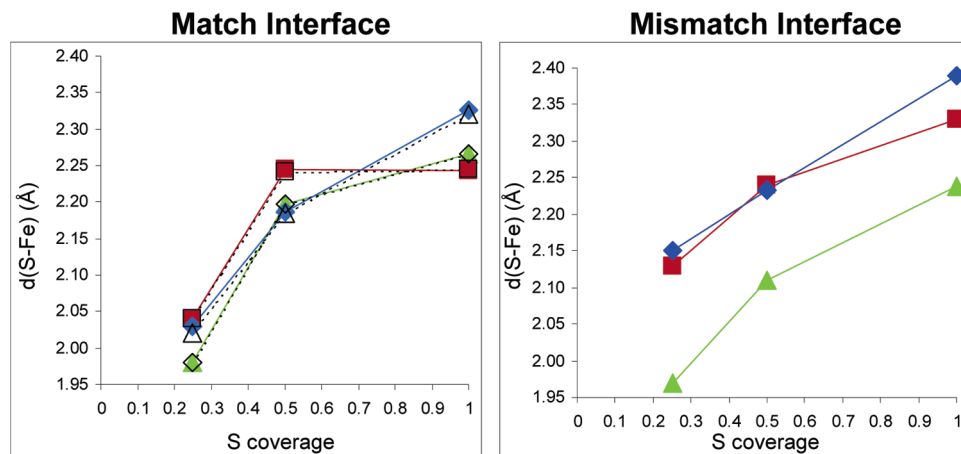


Figure 4. Calculated shortest S–Fe distances, $d(\text{S–Fe})$, of the relaxed matching and mismatching interfaces at equilibrium interfacial separation. Symbols as per Figure 2.

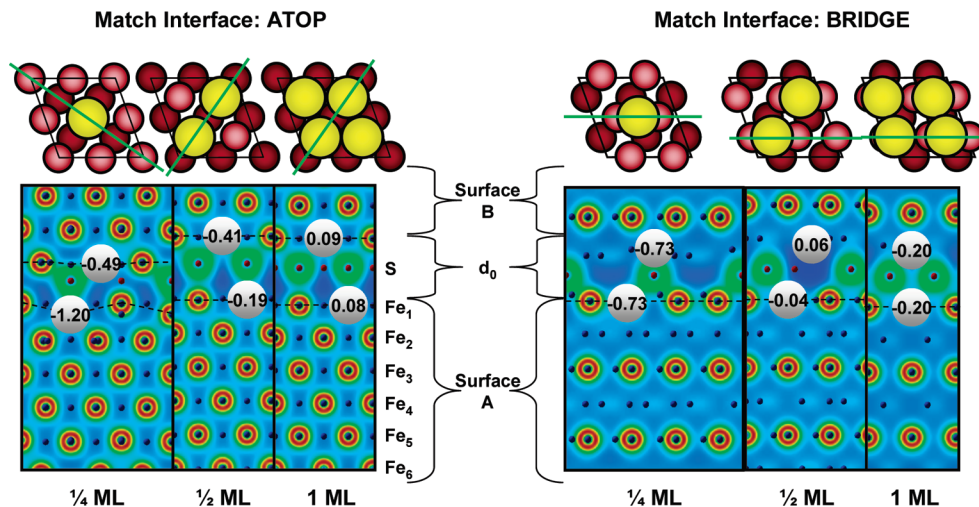


Figure 5. Charge density plots of atop and bridge matching interfaces with slices taken through the azimuths indicated. The calculated magnetic moment enhancement values, $\Delta\mu_B$, of the Fe atoms closest to the S atoms on either side of the interface are also indicated.

We previously compared the geometry of the 1/4 ML coverage S/Fe interfaces with some naturally occurring iron sulfide minerals.⁴ Such minerals include pyrite (FeS_2), marcasite (FeS_2), pyrrhotite (Fe_{1-x}S , where $0 < x < 0.2$), troilite (FeS), and smythite (Fe_3S_4), all varying in their stoichiometries and/or crystal structures.

While pyrite and marcasite have the same stoichiometry, they have different crystal arrangements. Pyrite has a cubic structure, based on the NaCl structure, where the Na ions are replaced with Fe, and the Cl anions are replaced with (S–S)²⁻ anion pairs. Marcasite, in contrast has an orthorhombic structure, but still contains the S–S pairs. Hence, in each structure, each Fe atom is surrounded by six S atoms in a distorted octahedron and each S atom is surrounded by one S atom and three nearest-neighbor Fe atoms in a distorted tetrahedral arrangement.

The structures of pyrrhotite, troilite, and smythite on the other hand, are all based on the NiAs structure. They all have a crystal structure that is layered, with alternating layers comprising only Fe or S atoms. This arrangement resembles that of our interfaces, where the layer of S atoms at the interface boundary is surrounded by a layer of Fe atoms on either side.

We compared the S–Fe and S–S distances found in these natural minerals with those of our interfaces. The S–Fe bond distances in the naturally occurring iron sulfide minerals have been found to vary slightly for different samples of the same mineral, but are generally around the following values: 2.259

Å²⁶ (pyrite), 2.213 or 2.243 Å²⁷ (marcasite), in the range 2.37–2.72 Å²⁸ (and references therein) (pyrrhotite), 2.36–2.72 Å²⁹ (troilite), and 2.386, 2.516, or 2.516 Å³⁰ (smythite). The shortest S–S distances have been determined to be 2.162 Å (pyrite), 2.241 Å (marcasite), 3.38–3.45 Å (pyrrhotite), 3.34 Å (troilite), and 2.768 Å (smythite).

In our different S-contaminated interfaces, we found the S–Fe distances to lie within the range 1.97–2.39 Å and the distance between adjacent S atoms to be 2.47, 2.86, or 4.95 Å, depending on the coverage. Hence, the overall similarity of the S–Fe geometries to those found in the naturally occurring minerals suggests that the bonding is of a similar nature.

The S–S separations in our interfaces at the 1/2 and 1 ML coverages were found to lie between the values for pyrite or marcasite and the values for smythite, pyrrhotite, and troilite. At 1/4 ML, the values are larger than all these iron sulfide minerals.

3.2.3. Charge Density. 3.2.3.1 Matching Interfaces. The charge density plots for the matching interfaces after relaxation at the equilibrium interfacial separation are shown in Figure 5. The charge density plots for the 4-fold hollow matching interfaces are not shown as the geometric analysis indicated these interfaces to be identical to the atop interfaces. The charge density slices are taken along the direction shown.

The rearrangement of charge density on both sides on the interface indicates the S bonds to both surface A and surface

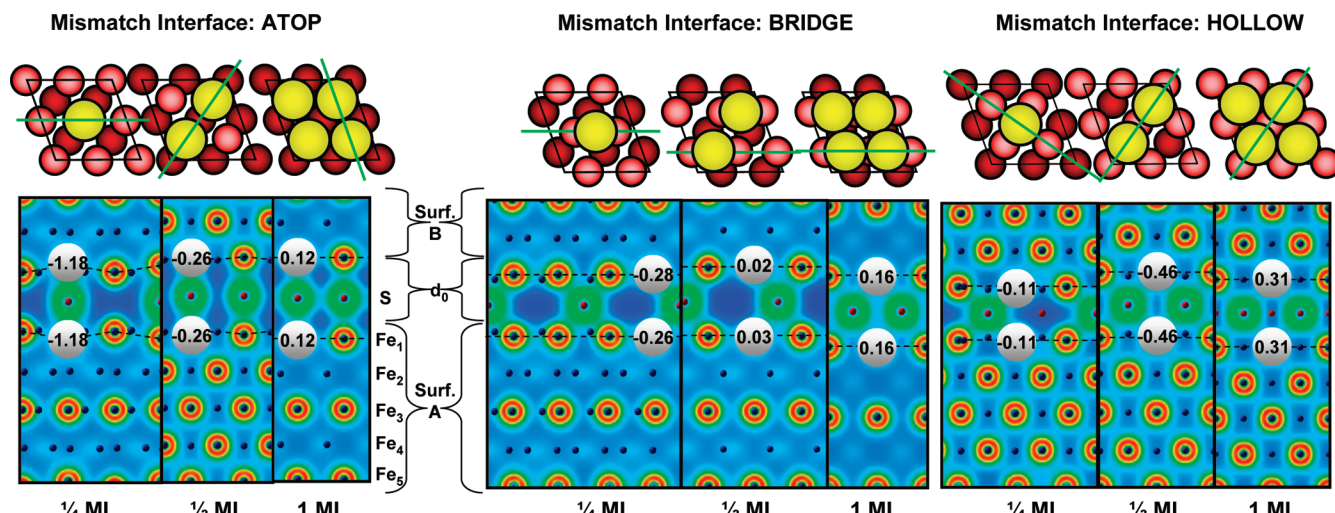


Figure 6. Charge density plots of the atop, bridge, and hollow mismatching interfaces with slices taken through the azimuths indicated. The calculated magnetic moment enhancements, $\Delta\mu_B$, of the Fe atoms closest to the S on either side of the interface are also indicated.

B, as was seen previously for the S-contaminated 1/4 ML coverage interfaces.⁴ In addition, comparison of the charge density plots of the interfaces in Figure 5 with those of the isolated S-contaminated surfaces^{16,23} shows that the S bonds to the same atoms as on the clean isolated surface: for an atop site the S bonds to the Fe atom directly below it; for a bridge site and a 4-fold hollow site the S bonds equally to the two closest Fe atoms, with these atoms being further apart for a 4-fold hollow site.

For the atop and 4-fold hollow matching interfaces, the S bonds to different sites on surfaces A and B. The charge density plots have been taken along slices that cut the shortest S–Fe bonds on both surfaces A and B, so it can be seen that S bonds directly to one Fe atom on surface A and two Fe atoms on surface B; i.e., the S is 3-fold bonded at this interface. At the higher coverages of 1/2 and 1 ML, some bonding between adjacent S atoms can also be seen; however, as the slices shown in Figure 5 are not taken along the shortest S–S direction for the 1 ML coverage, the trend of increasing S–S interaction with increasing coverage is not clearly seen. Slices taken along the shortest S–S direction do clearly show this trend, in line with that observed for the isolated surfaces.^{16,23}

In the earlier section on the geometry of the interfaces, it was discussed that the Fe atoms on surfaces A and B become buckled at the interface. This buckling was seen for all sites at 1/4 ML coverage and for the atop and 4-fold hollow sites at 1/2 ML coverage, where the Fe atoms not bonded directly to the S atoms move closer to each other across the interface, but not at 1 ML coverage.²³ This movement reduces the regions of low charge density, increasing the stability and strength of the interface. For the higher coverages we examined, all the Fe atoms along the slices shown are bonded directly to a S atom and hence have fewer degrees of freedom to move, showing little or no buckling at the interface.

For the bridge matching interfaces, the two Fe atoms that are bonded to the S on surface B are perpendicular to those on surface A and hence the slices presented in Figure 5 only show the S bonding to atoms on surface A. Slices taken perpendicular to these do confirm that the S bonds to two Fe atoms on surface B and hence is 4-fold bonded at this interface. In the 1 ML plot, where the slice coincides with the direction of the shortest S–S distance, the strong interaction between adjacent S atoms is clearly seen. From these plots it appears that the strength of

the interaction between the S and bonded Fe atoms decreases with increasing coverage.

3.2.3.2. Mismatching Interfaces. The charge density plots of the mismatching interfaces are shown in Figure 6. The slices are taken along the direction of the shortest S–Fe distances, unless otherwise indicated. It can be seen from the slices presented in Figure 6 that S forms bonds to both surface A and surface B and that the bonding is symmetric about the interface in line with the geometry at all S coverages. The S bonds to two atop sites, two bridge sites, or two 4-fold hollow sites for the atop, bridge, and 4-fold hollow interfaces, respectively, and is therefore 2-fold bonded in the atop interfaces and 4-fold bonded in the bridge and 4-fold hollow interfaces.

For the atop and 4-fold hollow interfaces, the buckling of the atoms at the interface can be seen at 1/4 and 1/2 ML S coverage. Similar to the matching interfaces, this buckling reduces the interfacial separation as well as the regions of low charge density at the interface, hence increasing the adhesive strength of the interface. The regions of low charge density at the mismatching interfaces, however, are still larger than for the corresponding matching interfaces, explaining the smaller adhesion energy values. The bridge interfaces also show large regions of low charge density at these coverages, with the charge density slices confirming for all the interfaces that they are symmetrical with equivalent bonding to the Fe atoms on surfaces A and B.

At 1 ML S coverage, the charge density plots for the bridge and 4-fold hollow interface indicate that the geometry is most similar to that of the clean matching Fe(110) interface, where the S atoms replace the middle layer Fe atoms. Due to steric hindrance, the S increases the interfacial separation, hence reducing the strength of adhesion, as was seen in the previous section. At these higher coverages the plots indicate that there are no direct Fe–Fe interactions across the interface.

3.2.4. Magnetic Moments. The magnetic moment enhancements, $\Delta\mu_B$, were determined for the Fe atoms directly bonded to the S atom on both sides of the interface. They are determined by subtracting the previously calculated magnetic moment value, μ_B , of 2.40 μ_B for bulk Fe,³¹ from the μ_B of the topmost surface Fe atoms directly bonded to the adsorbed S atom and are shown on the charge density plots for the matching and mismatching interfaces in Figures 5 and 6.

3.2.4.1. Matching Interfaces. Comparison of the $\Delta\mu_B$ values of the atop and 4-fold hollow matching interfaces further confirm that these interfaces are identical after relaxation; the $\Delta\mu_B$ of the Fe atoms bonding to atop or 4-fold hollow sites on surfaces A and B, respectively, in the atop interfaces were identical to the corresponding surfaces on the 4-fold hollow interfaces at the same coverage. Therefore, only the atop interface values are shown in Figure 5. The μ_B enhancements for the Fe atoms bonded to the atop site on surface A are not, however, identical to those on surface B, where S bonds in a 4-fold hollow site, as might be expected due to the different degrees of coordination of the Fe atoms in these sites. For S bonding to an atop site, the μ_B enhancement at the lowest coverage is negative. As the coverage is increased, the magnitude of the μ_B enhancement decreases, resulting in a slightly positive value at monolayer coverage. This indicates that at the lower coverages the S causes spin pairing, reducing the absolute magnetic moment values of the Fe atoms, while at higher coverages, where the ratio of S to Fe atoms at the interface is greater, there is less spin pairing and hence larger magnetic moment values are observed. The trend in $\Delta\mu_B$ values of the interfaces at the different coverages does not follow that seen for the isolated S-contaminated surfaces, indicating the effect the formation of the interface has on the magnetic properties.

For S bonding in a 4-fold hollow site (surface B) the $\Delta\mu_B$ values are also negative at coverages below 1 ML but are almost the same as the atop site values at 1 ML, where they are close to zero. This indicates that the magnetic moment values are almost the same as those for bulk Fe and are similar to the values at the clean matching interface, where the μ_B enhancements were essentially zero as the atoms are arranged as they are in the bulk structure.

For the bridge site, where the S is located between two bridge sites, the μ_B enhancements are the same on surface A as they are on surface B for the 1/4 and 1 ML interfaces. At the intermediate coverage, the magnetic moment enhancement values are slightly different on surfaces A and B; however, this difference is only $0.1\mu_B$. Similar to the atop/4-fold hollow interfaces, the values generally become positive at the higher coverage. For the bridge interfaces, though, the enhancements are essentially zero at 1/2 ML, but then become negative again at 1 ML.

It was shown in section 3.2.1 that the adhesion energy of the relaxed matching interfaces varied between 1.15 and 2.57 J m^{-2} . Comparison of the E_0 values with the nature of the μ_B enhancements indicates that the interfaces that display bulk-like magnetic moment values have intermediate adhesion energy values. The interfaces are strongest when the S is found to reduce the Fe magnetic moment values below that of the bulk.

3.2.4.2. Mismatching Interfaces. For the mismatching interfaces (Figure 6), the symmetry-equivalent atoms (by geometry) are found to have the same μ_B enhancement values. Again, in general, the $\Delta\mu_B$ values depend on the degree of S–Fe coordination at the interface. The μ_B enhancements are all negative at the lowest S coverage and are found to become positive at the higher coverages, similar to the trend seen for the matching interfaces.

4. Conclusion

The findings from this study have shown that S reduces the adhesive strength of Fe(110) surfaces in match and mismatch orientations at all coverages examined (1/4, 1/2, and 1 ML).

For the matching configuration, the atop interface with 1/2 ML S coverage is found to have the largest work of separation.

For the mismatching configuration, the bridge 1/2 ML mismatching interface, while still being weaker than the strongest matching interface, has the largest work of separation. The mismatching 4-fold hollow 1 ML interface has such a low work of separation that it is unlikely to form.

At the S coverages examined, the interfacial separation was increased by the presence of the S, as compared to the clean interfaces. The distance of the S from the two surfaces forming the interface was found to be directly related to the type of adsorption site it sits in at the two surfaces and the relative heights of the relaxed S atom on the isolated surface. The calculated peak interfacial stress values were generally in line with the calculated work of separation values as there was little difference in the calculated screening length values.

Relaxation of the interfaces around their equilibrium separation was found to lead to an increase in the adhesion energy, which was not large enough to make them stronger than the clean matching or mismatching interfaces. Of all the contaminated interfaces examined, the strongest matching interface was still the one with S adsorbed in atop sites at 1/2 ML coverage, while the strongest mismatching interface became the interface with the 1/4 ML coverage and S adsorbed in hollow sites.

The geometry of the relaxed interfaces was related to the height of the adsorbed S atom on the isolated surface. The charge density plots were in line with the geometry analysis, indicating that the S bonds to the closest Fe atoms on both sides of the interface. The magnetic moment values calculated for the relaxed interfaces indicated that the interfaces with magnetic moment enhancement values closer to those of the clean interfaces only showed intermediate adhesive strength.

Acknowledgment. The Victorian Partnership for Advanced Computing (VPAC) and Australian Partnership for Advanced Computing (APAC) are acknowledged for provision of computer facilities.

References and Notes

- (1) Buckley, D. H. *Int. J. Nondestructive Test.* **1970**, 2, 171.
- (2) Hung, A.; Yarovsky, I.; Muscat, J.; Russo, S.; Snook, I.; Watts, R. O. *Surf. Sci.* **2002**, 501, 261.
- (3) Spencer, M. J. S.; Hung, A.; Snook, I. K.; Yarovsky, I. *Surf. Sci.* **2002**, 515, L464.
- (4) Spencer, M. J. S.; Snook, I. K.; Yarovsky, I. *J. Phys. Chem. B* **2004**, 108, 10965.
- (5) Hartweck, W.; Grabke, H. J. *Surf. Sci.* **1979**, 89, 174.
- (6) Hartweck, W. G.; Grabke, H. J. *Acta Metall.* **1981**, 29, 1237.
- (7) Rose, J. H.; Smith, J. R.; Ferrante, J. *Phys. Rev. B* **1983**, 28, 1835.
- (8) Finnis, M. W. *J. Phys.* **1996**, 8, 5811.
- (9) Dupre, A. *Theorie Mechanique de la Chaleur*; Gauthier-Villars: Paris, 1869.
- (10) Kresse, G.; Hafner, J. *Phys. Rev. B* **1993**, 48, 13115.
- (11) Kresse, G.; Furthmuller, J. *Comput. Mater. Sci.* **1996**, 6, 15.
- (12) Kresse, G.; Furthmuller, J. *Phys. Rev. B* **1996**, 54, 11169.
- (13) Kohn, W.; Sham, L. J. *Phys. Rev.* **1965**, 140, 1133.
- (14) Perdew, J. P.; Yue, W. *Phys. Rev. B* **1992**, 45, 13244.
- (15) Monkhorst, H. J.; Pack, J. D. *Phys. Rev. B* **1976**, 13, 5188.
- (16) Spencer, M. J. S.; Hung, A.; Snook, I.; Yarovsky, I. *Surf. Sci.* **2003**, 540, 420.
- (17) Vanderbilt, D. *Phys. Rev. B* **1990**, 41, 7892.
- (18) Spencer, M. J. S.; Hung, A.; Snook, I. K.; Yarovsky, I. *Surf. Sci.* **2002**, 513, 389.
- (19) Spencer, M. J. S.; Hung, A.; Snook, I.; Yarovsky, I. *Surf. Rev. Lett.* **2003**, 10, 169.
- (20) Muscat, J.; Hung, A.; Russo, S.; Yarovsky, I. *Phys. Rev. B* **2002**, 65, 054107/1.
- (21) Hung, A.; Muscat, J.; Yarovsky, I.; Russo, S. P. *Surf. Sci.* **2002**, 520, 111.
- (22) Hung, A.; Muscat, J.; Yarovsky, I.; Russo, S. P. *Surf. Sci.* **2002**, 513, 511.
- (23) Spencer, M. J. S.; Snook, I. K.; Yarovsky, I. *J. Phys. Chem. B.*, in press.

- (24) Methfessel, M.; Paxton, A. T. *Phys. Rev. B* **1989**, *40*, 3616.
- (25) Blochl, P. E.; Jepsen, O.; Andersen, O. K. *Phys. Rev. B* **1994**, *49*, 16223.
- (26) Finklea, S. L.; Cathey, L.; Amma, E. L. *Acta Crystallogr., Sect. A* **1976**, *32*, 529.
- (27) Buerger, M. J. *Am. Mineral.* **1931**, *16*, 361.
- (28) Mikhlin, Y. L.; Tornashevich, Y. V.; Pashkov, G. L.; Okotrub, A. V.; Asanov, I. P.; Mazalov, L. N. *Appl. Surf. Sci.* **1998**, *125*, 73.
- (29) King, H. E.; Prewitt, C. T. *Acta Crystallogr., Sect. B: Struct. Sci.* **1982**, *38*, 1877.
- (30) Evans, H. T. J.; Erd, R. C. *American Crystallographic Association: Program Summer 1955*; 1955; p 14.
- (31) Yarovsky, I.; Spencer, M. J. S.; Snook, I. K. Iron surfaces and interfaces: structure and properties from Density Functional Theory. In *Progress in Surface Science Research*; Columbus, F., Ed.; Nova Science Publishers: Hauppauge, NY, 2005; in press.